IMPROVED SEGMENTATION OF MR BRAIN IMAGES INCLUDING BIAS FIELD CORRECTION BASED ON 3D-CSC*

Haojun Wang, Patrick Sturm, Frank Schmitt, Lutz Priese

Institute for Computational Visualistics, University of Koblenz-Landau, 56070 Koblenz, Germany

Keywords: Image segmentation, 3D Cell Structure Code, MRI, Brain, Classification.

Abstract: The 3D Cell Structure Code (3D-CSC) is a fast region growing technique. However, directly adapted for segmentation of magnetic resonance (MR) brain images it has some limitations due to the variability of brain anatomical structure and the degradation of MR images by intensity inhomogeneities and noise. In this paper an improved approach is proposed. It starts with a preprocessing step which contains a 3D Kuwahara filter to reduce noise and a bias correction method to compensate intensity inhomogeneities. Next the 3D-CSC is applied, where a required similarity threshold is chosen automatically. In order to recognize gray and white matter, a histogram-based classification is applied. Morphological operations are used to break small bridges connecting gray value similar non-brain tissues with the gray matter. 8 real and 10 simulated T1-weighted MR images were evaluated to validate the performance of our method.

1 INTRODUCTION

Segmentation of 3D MR brain images is an important procedure for 3D visualization of brain structures and quantitative analysis of differences between normal and abnormal brain tissues. Up to now many segmentation techniques have been developed (Suzuk 1991, MacDonald 2000, Zhang 2001, Stokking 2000, Schnack 2001). However, most intensity-based schemes fail to segment MR brain images into gray and white matter satisfactorily due to the effect of intensity inhomogeneities (also referred as bias field) (Rajapakse 1998, Wells III 1996, Sled 1998) resulting from irregularities of the scanner magnetic fields, radio frequency, etc. The deformable-based techniques sometimes do not converge well to the boundary of interest due to the complicated deformations in the anatomy (Pham 2000). Furthermore existing fully automatic segmentation techniques have to make a compromise between speed and accuracy of processes in practice. Therefore, an automatic robust and fast 3D brain segmentation method is needed that is able to detect gray and white matter.

A 3D hierarchical inherently parallel region growing method, called 3D-CSC, has recently been developed in our group and at Research Centre Juelich. It is an effective 3D generalization of the 2D-CSC (Priese 2005). In comparison with traditional region growing techniques it does not depend on the selection of seed points. It is very fast due to its hierarchical structure. The advantages of the technique are local simplicity and global robustness. Therefore, we adapt the 3D-CSC for segmentation of 3D MR brain images. In the 3D-CSC, region growing is steered by a hierarchical structure of overlapping cells. Overlapping and gray-similar regions in one hierarchy level are merged to a new region of the next level. Unfortunately some known difficulties in MR brain images, such as intensity inhomogeneities and the effect of noise, degrade the performance of 3D-CSC segmentation. This results in an over-segmentation. In order to overcome these difficulties, a preprocessing step which includes a 3D Kuwahara filter to reduce random noise and a correction of intensity inhomogeneities is applied. In addition, a postprocessing step based on histogram-based classification of CSC segments and morphology-based shape constraints is integrated in our scheme. All processing steps are fully automatic.

The paper is organized as follows: Section 2 briefly introduces 3D-CSC segmentation. Section 3

describes the improved segmentation scheme for brain images. Experimental results and conclusion are given in Section 4 and Section 5 respectively.

2 3D CELL STRUCTURE CODE

The 3D-CSC steers a hierarchical region growing on a special 3D topology. In order to understand this hierarchy we first introduce the hierarchical hexagonal topology (see Figure 1(a)) of the 2D–CSC (Rehrmann 1998). The topology is formed by so called islands in different levels. An island of level 0 consists of a center pixel and its six neighboring pixels. An island of level n+1 consists of a center island of level n and its six neighboring islands of level n. Two neighboring islands of level n overlap in a common island of level n-1. This is repeated until one big island covers the whole image. In order to apply the hierarchical topology in a real image, the hexagonal island structure is transformed logically to an orthogonal grid as shown in Figure 1(b).

Generalizing the 2D hierarchical hexagonal topology to 3D forms the 3D hierarchical cell topology. It is constructed by the densest sphere packing (see Figure 2(a)). Here we just focus on the S_{15} cell structure (see Figure 2(b) and 2(c) where 2(c) is a transformation into the orthogonal 3D grid.). In S_{15} a cell of level 0 consists of 15 voxels (1 center voxel and its 14 neighboring voxels).

The S_{15} cell structure possesses the following properties:
• 14-neighborhood: each cell of level n overlaps with 14 cells of level n.
• Plainness: two cells of level n+1 overlap each other in at most one cell of level n.
• Coverability: each cell (except the topmost one) of level n is a sub-cell of a parent cell of level n+1.
• Strong Saturation: all sub-cells (except the center cell) of a cell of level n+1 are sub-cells of exactly two different cells of level n+1. Each center cell has exactly one parent cell.

These properties lead to a nice and efficient implementation. Also the information about location and neighborhood of each cell can be derived quickly. In the 3D-CSC, region growing is done independently in each cell of each level. Neighboring and similar segments in lower levels will be merged to bigger segments in a higher level. If two neighboring segments are dissimilar they will be split. For a deeper discussion see (Sturm 2004). Here 'similar' means the difference of the mean intensity of two neighboring segments is

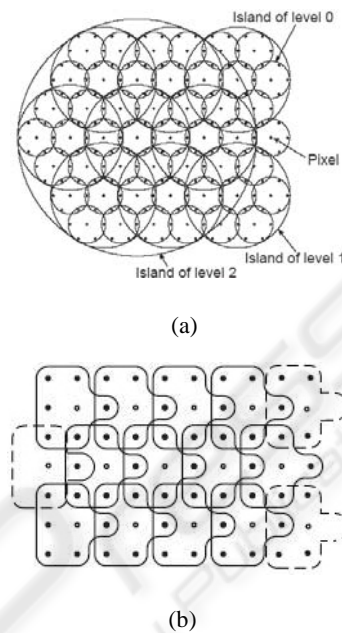below a certain threshold T. The threshold T will be chosen automatically.

(a)

(b)

Figure 1: The hierarchical hexagonal island structure and its deformation on the orthogonal grid.
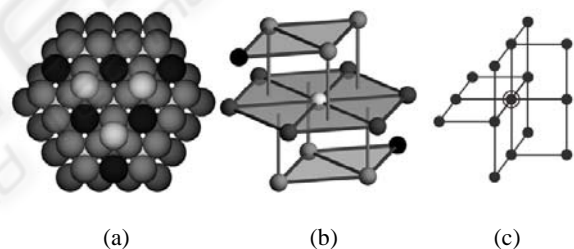

(a)   (b)   (c)

Figure 2: 3D hierarchical cell topology and S_{15} cell structure.

3 ADAPTION TO BRAIN IMAGES

The segmentation procedure for 3D MR brain images consists of three parts:
• Preprocessing: noise suppression and bias field correction. (Described in section 3.1)
• 3D-CSC segmentation. (General case described in section 2, adaption to MR brain images described in section 3.3)
• Postprocessing: classifying the primitive CSC segments into brain and non–brain tissues, then breaking small connections between them and separating brain tissue into gray and white matter. (Described in section 3.4)

339

3.1 Preprocessing: Filter and Bias Field Correction

To reduce noise, we apply a 3D generalization of the Kuwahara filter as it gives a very good tradeoff between performance and speed and has been proved to be an ideal nonlinear filter for smoothing regions and preserving edges (Kuwahara 1976).

Recently a successful method for dealing with the bias field problem has been proposed (Vovk 2004). The idea behind it is to iteratively sharpen probability distributions of image features along intensity features by an intensity correction force. Then the bias correction estimation is calculated. This correction method combines intensity and spatial information and estimates the intensity inhomogeneity on each image point.

The following notations are given:

- V is the number of voxels in an image
- x is the three dimensional location of a voxel
- $u(x)$ is the measured gray value at the location x in a MR image
- $v(x)$ is the ideal gray value in the absence of any bias field
- $n(x)$ is noise at location x
- $f(x)$ is the bias field at x
- $d_u = L(u)$ is the Laplacian (2nd derivative) of u
- P_u is the probability distribution (2 dim. histogram) of u and d_u, where $P_u(a,b) = n$ tells that exactly n voxels $x_1 \dots, x_n$ have the values $u(x_i) = a$ and $d_u(x_i) = b$
- $\mu_{|F|}$ is the mean value of the set of the absolute force $|F|$

(Vovk 2004) considers the usual model of image formation in MR as:

$$u(x) = v(x) \cdot f(x) + n(x) \qquad (1)$$

$n(x)$ is neglectable as we have already applied a Kuwahara filter to reduce noise. First set $u_1 := u$, then apply the following iteration (2)-(4):

$$F_i = \frac{1}{V} \cdot \frac{\partial}{\partial a} (\ln P_{u_i}) \qquad (2)$$

F_i are the correction forces and are derived by the weighted partial derivate of logarithm of P_{u_i} along the intensity value a (the first coordinate of P_{u_i}), then are mapped to the points with corresponding features in the image.

$$f_i^{-1} = 1 + \frac{k}{\mu_{|F_i|}} \cdot G(F_i) \qquad (3)$$

where G is a three dimensional Gaussian filter and carries out a convolution with F_i, k is a pre-chosen parameter.

In the principle, the corrected image v_i at iteration i and the input image u_{i+1} at iteration $i+1$ are expressed as:

$$u_{i+1} = v_i = u_i \cdot f_i^{-1} = u \cdot \prod_{j=1}^{i} f_j^{-1} \qquad (4)$$

However in practice, preserving the brightness of the original input image u must be taken into account in each iterative correction (More details are described in (Vovk 2004)). No automatic termination criterion for the iterations is proposed in (Vovk 2004). Hence we focus on this and consider the mean of absolute variation D_i (see equation (6)) which reflects the changes between the overall estimated bias correction $\hat{f}_i^{-1}$ after iteration i and the initial correction $\hat{f}_0^{-1} = 1$.

$$\hat{f}_i^{-1} = \frac{\mu_u}{\mu_{u_i^*}} \cdot \prod_{j=1}^{i} f_j^{-1} \approx \frac{\mu_u}{\mu_{u_i^*}} \cdot \hat{f}_{i-1}^{-1} \cdot f_i^{-1} \qquad (5)$$

$$D_i = \mu_{\left| \hat{f}_i^{-1} - \hat{f}_0^{-1} \right|} \qquad (6)$$

In (5), $\hat{f}_i^{-1}$ will be used to correct the original input image u, then the corrected image v_i is derived, μ is the mean value, u_i^* is expressed by:

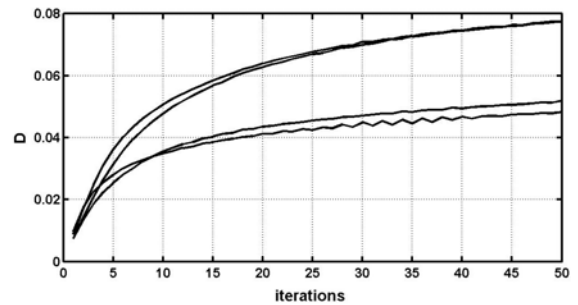$$u_i^* = u \cdot \hat{f}_{i-1}^{-1} \cdot f_i^{-1} \qquad (7)$$

Figure 3: D_i curves for several tested images.

Figure 3 shows several typical curves of D_i for tested images. D_i increases and tends to roughly converge, although some small vibrations exist locally. Images with low inhomogeneities converge faster than those with high inhomogeneities. This means images with low inhomogeneities need less iterations for the correction. Thus a termination

criterion will be derived, i.e. in each 5 iterations we compute the regressive straight line of D_i, if the slope coefficient of the regressive straight line is below a termination threshold E the iteration will stop otherwise continue. The purpose of the regressive straight line is to eliminate the effect of small local vibrations of D_i. This has been proved to be robust in our tested images. With the same constraint E the iterative corrections of all tested images will stop after 10-25 steps according to their degree of inhomogeneity .

To reduce computational cost for the Gaussian convolution in equation (3), the MR data is down-sampled by factor 3 in each dimension. The degradation of performance is neglectable, because the bias field varies just slowly across an image.

As the background is not degraded by the bias field and could interfere with the estimation, it is removed prior to our correction method automatically.

3.2 Histogram Analysis

Histogram analysis plays an important role in our method: We use it to detect the similarity threshold for 3D-CSC segmentation and for classification after the CSC. Image histograms contain information about intensity distributions of tissues in MR images. We here only consider T1 weighted MR brain images. The histograms of those images normally contain five modes, listed from dark to bright: background, cerebrospinal fluid (CSF), gray matter (GM), white matter (WM) and fat. The spatial variations of the same tissue class and the effect of bias field make them overlap each other. After bias field correction the overlapping between classes is reduced. This enables us to recognize them in intensity space, i.e. to find thresholds that separate those classes by their intensities.

First we consider the intensity histogram h of the preprocessed image as a Gaussian mixture model (GMM) (see (8)-(9)), where each Gaussian represents the intensity distribution of each tissue class in an MR image. The approximated normalized histogram $\hat{h}$ is expressed by:

$$\hat{h} = \sum_{i=1}^{C} \hat{a}_i \cdot G_{\hat{\mu}_i, \hat{\sigma}_i} \qquad (8)$$

C is the number of Gaussians, $\hat{a}_i$, $\hat{\mu}_i$ and $\hat{\sigma}_i$ are the estimated mixing weight, mean and standard deviation of the i-th Gaussian which is given by:

$$G_{\hat{\mu}_i, \hat{\sigma}_i}(g) = \frac{1}{\sqrt{2\pi}\hat{\sigma}_i} \exp\left[\frac{-(g - \hat{\mu}_i)^2}{2 \cdot \hat{\sigma}_i^2}\right] \qquad (9)$$
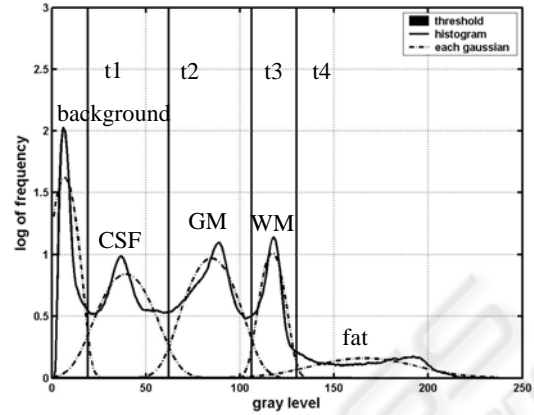
where g is a gray level.

Figure 4: The result of histogram analysis.

To obtain the parameters of the Gaussian mixture model we follow the scale space filtering method of (Carlotto 1987). This gives us a good initialization for $\hat{a}_i$, $\hat{\mu}_i$, and $\hat{\sigma}_i$. With the Expectation-Maximization (EM) algorithm (Duda 2001), those parameters are further refined.

The result of the GMM estimation for a sample image and the thresholds separating the five classes for later classification are shown in Figure 4 where each Gaussian contains the mixing weight. We refer to the threshold between background and CSF as t1, between CSF and gray matter as t2, between gray and white matter as t3 and between white matter and fat as t4.

3.3 Adaption of the 3D-CSC for MR Brain Images

As mentioned in section 2, the 3D-CSC requires a similarity threshold T. As there is no constant value for T applicable for all MR images, we developed an automatic method for finding a reasonable value based on the histogram analysis method described in section 3.2. T is derived by computing the shortest distance D_s between the centers of two estimated Gaussians in the histogram of the corrected image. T is equal to D_s divided by 4 which proved to result in near-optimal values for MR brain images from various sources.

3.4 Postprocessing

The 3D-CSC segmentation does not result in a single segment for gray resp. white matter. Instead gray and white matter are oversegmented and

sometimes parts of gray matter and non-brain tissues are merged to one segment due to narrow gray value bridges. Therefore some postprocessing steps are needed: First the CSC segments are preliminary classified in brain and non-brain by their mean gray value (see 3.4.1). As only the mean gray value is considered segments containing non-brain tissues with an intensity similar to gray or white matter are classified always as brain. This problem is solved by morphological operations (see 3.4.2). Finally the brain is separated into gray and white matter.

3.4.1 Preliminary Classification

We obtain a preliminary brain mask by doing a classification of CSC segments in which we use the intensity thresholds (see section 3.2) to select all segments which could belong to the brain. I.e. if the mean intensity of a segment belongs to the range [t2, t4] the segment should be kept in the preliminary brain mask otherwise discarded. However, even if optimal thresholds are used, connections between the brain and surrounding non-brain tissues still occur. In order to break these connections and reduce misclassification, morphological operations are applied.

3.4.2 Morphological Operations and Final Classification

We apply the following morphological operations to break up bridges between brain and non-brain tissues:
- Select the largest connected component (LCC1) in the preliminary brain mask and perform an erosion with a ball structuring element with radius of 3-5 voxels (depending on the size of the input image). This breaks connections between the brain and non-brain tissues.
- Select the largest connected component (LCC2) after the erosion and perform a dilation with the same size structuring element to get LCC3. This reconstructs the eroded brain segment.
- Compute the geodesic distances to LCC3 from all points which only belong to LCC1 but not to LCC3 using a 1 voxel radius ball structuring element. Then assign all points whose distances are <= 4 voxels to LCC3 as the final segmented brain. In this step some more detailed structures of the segmented brain are recovered

At last, we remove all voxels not belonging to the brain mask from the CSC segments. The threshold t3 is then applied to classify the remaining segments into gray matter (GM) and white matter (WM).

4 EXPERIMENTS AND RESULTS

To assess the performance of the proposed method, we applied it to 18 T1-weighted MR brain images (10 simulated images and 8 real images). The simulated images were downloaded from the Brainweb site (http://www.bic.mni.mcgill.ca/brainweb). These images consist of 181x217x181 voxels sized 1x1x1mm with a gray value depth of 8 bits. 1%, 3%, 5%, 7% resp. 9% noise levels have been added and intensity inhomogeneity levels ("RF") are 20% and 40%. The real images were acquired at 1.5 Tesla with an AVANTO SIEMENS scanner from the BWZK hospital in Koblenz, Germany. They consist of 384x512x192 voxels with 12 bits gray value depth. The voxels are sized 0.45x0.45x0.9mm.

All processes were performed on an Intel P4 3GHz-based system. The execution time of the complete algorithm is about 24 seconds for a 181x217x181 image.

Some parameters need to be set for the bias field correction: The factor k in equation (3) which controls the speed of iterative correction, was set to 0.05. The standard deviation of the Gaussian filter determines the smoothness of correction. For the simulated images it was set to 30 for each dimension, but for the real images due to the anisotropic voxel resolution to 60x60x30. The termination threshold E of the bias field correction was set to 0.001 which automatically determines the iterations according to the degree of inhomogeneity and ensures the accuracy of correction. Figure 5 shows a correction example of a simulated image. The intensities of voxels belonging to the same tissue become relatively homogeneous in the corrected image (see Figure 5(b)). The misclassified part of the white matter (see Figure 5(e)) in the segmentation without bias field correction is recovered in the segmentation with bias field correction (see Figure 5(f)).

The Brainweb site provides the "ground truth" for the simulated images that enables us to evaluate the proposed method quantitatively. We use the following evaluation measures:
- Coverability Rate (CR) is the number of voxels in the segmented object (S) that belong to the same object (O) in the "ground truth", divided by the number of voxels in O.
- Error Rate (ER) is the number of voxels in S that do not belong to O, divided by the number of voxels in S.
- Similarity Index (SI) (Stokking 2000) is two times the number of voxels in the segmented object (S)

that belong to the same object (O) in the "ground truth", divided by the number of voxels both in S and O. SI is 1 for a perfect segmentation.

(a) uncorrected (b) corrected

(c) real bias field (d) estimated bias field

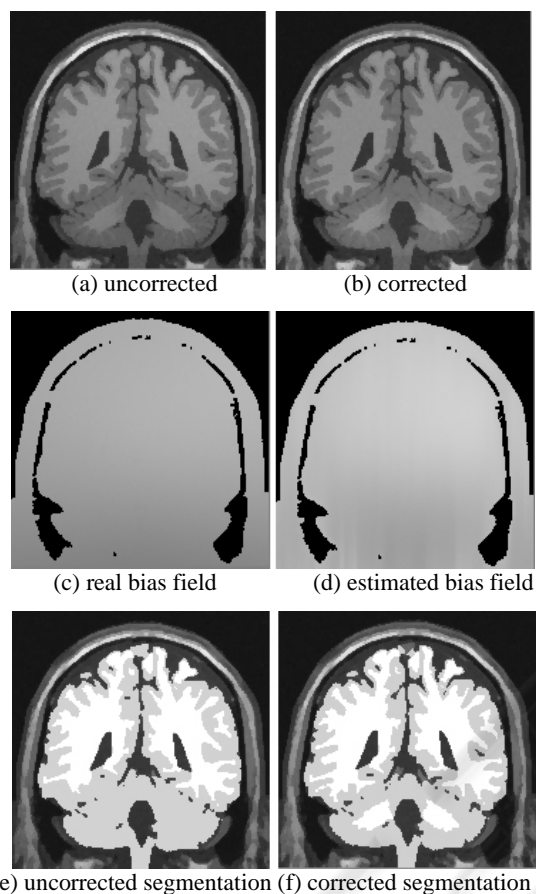(e) uncorrected segmentation (f) corrected segmentation

Figure 5: Comparison of the results of uncorrected and corrected simulated images (noise level=3%, RF=40%, filtered).

The evaluations of the uncorrected (UNC) and corrected (COR) simulated images with RF=20% and with RF=40% are shown in Figure 6, where CR, ER and SI are the average of GM and WM respectively. They show that the bias correction improved the performance of segmentation. After bias correction the intensity inhomogeneities in the images are compensated effectively both in RF=20% and RF=40%. In addition, the results of our method are compared with those from a popular brain analysis technique called Statistical Parametric Mapping (SPM) (Ashburner 2000). The software package SPM2 was released in 2003 (http://www.fil.ion.ucl.ac.uk /spm/) and a procedure for bias correction has been included. The comparison (see Figure 7) indicates that our method is comparable with SPM2. SPM2 uses an anatomical atlas. Our method does not depend on such an atlas and overcomes SPM2 for the noise levels 1%, 7% and 9%. For the noise levels 3% and 5% SPM2 shows only slightly better results.

Unfortunately for real images the 'ground truth' is not available, so the same quantitative measurement can not be conducted on them. Therefore we only visually evaluated them. The results with bias correction and without bias correction are compared. There are no big differences between them except for detailed structures which can be detected by using bias correction. In this paper we provide a segmentation example of a real image with and without bias correction (see Figure 8). The result with bias correction seems to be appreciably better on some detailed structures which are sketched out by circles. Its 3D visualization result is also shown in Figure 8.
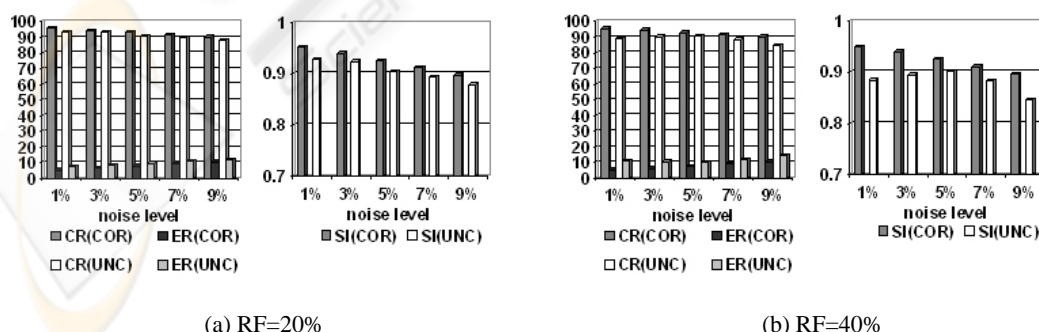

(a) RF=20% (b) RF=40%

Figure 6: Quantitive evaluation for the segmentation results of uncorrected and corrected simulated images.
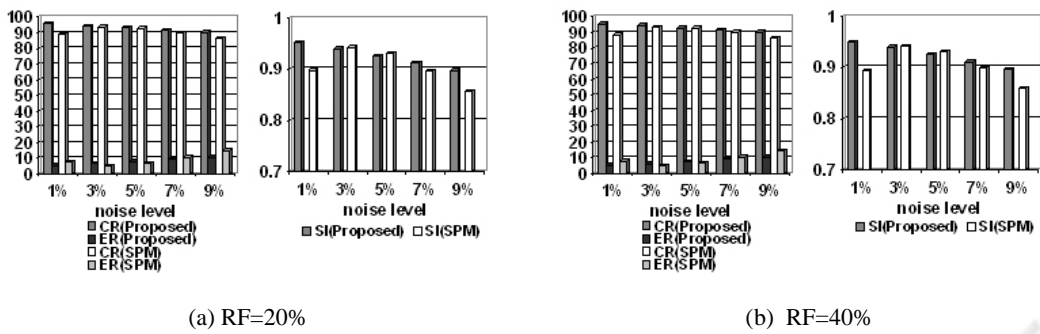
(a) RF=20%   (b) RF=40%

Figure 7: Quantitative evaluation for the segmentation results of simulated images comparing the proposed method with SPM2.
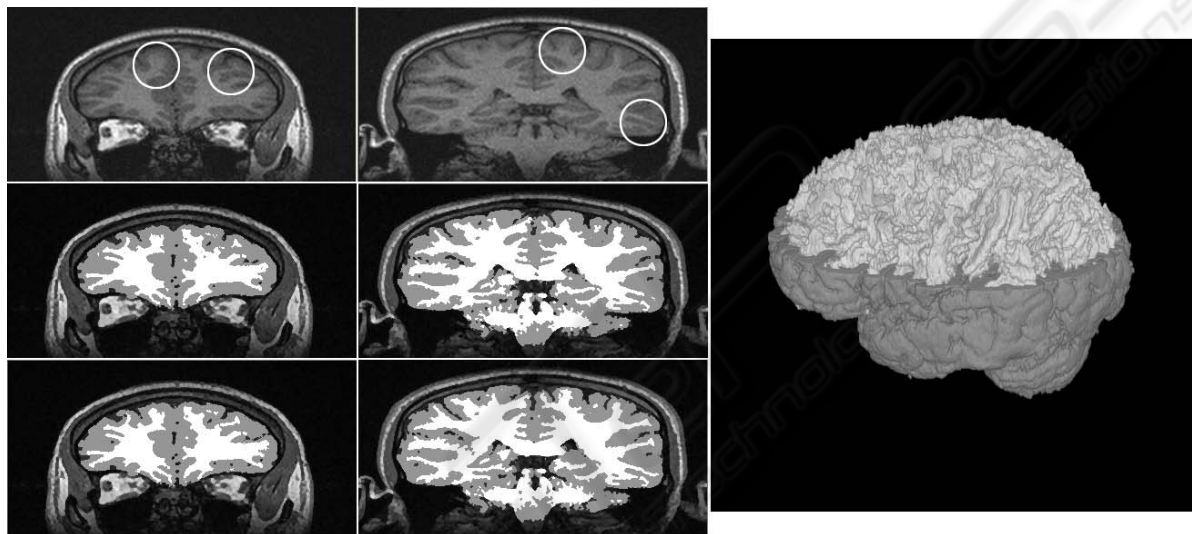

Figure 8: Comparison of the segmentation results of a real image with bias correction and without bias correction and its 3D visualization. The original slices are in the first row. The segmentation results without bias correction are shown in the second row. The third row shows the results with bias correction. Its 3D visualization is in the right column where the gray matter is partially removed.

5 CONCLUSION

A fully automated, improved segmentation based on the 3D-CSC for MR brain images is proposed in this paper. In contrast to most existing methods, it is fast with a satisfactory accuracy. It takes advantage of the region- and intensity-based 3D-CSC and combines it with further information from intensity histograms to robustly segment MR brain images. A bias correction is integrated into the method to improve its performance. However, the results for some images still indicate some problems: On the one hand some detailed structures of the brain are lost especially in the cerebellum, on the other hand we sometimes are not able to remove all non-brain tissues, i.e. sometimes small parts of non-brain

tissue around the eyes is still included. Those problems depend on the size of the structuring element of the morphological operations. A big structuring element can avoid including more non-brain tissues but some detailed structures of brain may be lost and vice versa.

In the future we have to cope with the above problems and want to segment and recognize other significant structures in 3D MR brain images. Furthermore, we want to compare our method with other state of art brain segmentation techniques, i.e. the Hidden Markov Random Field (HMRF)-based method (Zhang 2001), and the fuzzy C-means clustering (FCM)-based adaptive method (Liew 2003).

REFERENCES

Ashburner, J., Friston, K. J., 2000. Voxel-based morphometry-the methods. *NeuroImage.* 11(6Pt1): 805-821.

Carlotto, M. J., 1987. Histogram analysis using a scale-space approach, *IEEE Trans on PAMI.* 9(1): 121-129.

Duda. R. O., Hart, P. E., Stork, D. G., 2001. *Pattern Classificatio*, Wiley&SONS Press. London. 2nd edition.

Kuwahara, M., Hachimura, K., Eiho, S., 1976. Processing of Ri-angiocardiographic images. *Digital Processing of Biomedical Images*. Plenum Press. New York.

Liew, A. W., Yan, H., 2003. An adaptive spatial fuzzy clustering algorithm for 3-D MR image segmentation. *IEEE Trans on Medical Imaging.* 22(9): 1063-1075.

MacDonald, D., Kabani, N., Avis, D., 2000. Automated 3-D extraction of inner and outer surfaces of cerebral cortex from MRI. *Neuroimage.* 12(3): 340-356.

Pham, D. L., Xu, C. Y., Prince, J. L., 2000. Current methods in medical image segmentation, A*nnual Review of Biomedical Engineering.* 2: 315-337.

Priese, L., Sturm, P., Wang, H. J., 2005. Hierarchical Cell Structures for Segmentation of Voxel Images. In SCIA2005, *14th Scandinavian Conference on Image Analysis*. Springer Press.

Rajapakse, J. C., Kruggel, F., 1998. Segmentation of MR images with intensity inhomogeneities. *Image Vision Computing*. 16(3): 165-180.

Rehrmann, V., Priese, L., 1998. Fast and robust segmentation of natural color scenes. *In ACCV98. 3rd Asian Conference on Computer Vision.* Springer Press.

Schnack, H. G., Hulshoff Pol, H. E., Baare, W. F., 2001. Automated separation of gray and white matter from MR images of the human brain, *Neuroimage*. 13(1): 230-237.

Sled, J. G., Zijdenbos, A. P., Evans, A. C., 1998. A nonparametric method for automatic correction of intensity nonuniformity in MRI data. *IEEE Trans on Medical Imaging*. 17(1): 87-97.

Stokking, R., Vincken, K. L., Viergever, M. A., 2000. Automatic morphology-based brain segmentation (MBRASE) from MRI-T1 Data. *NeuroImage*. 12(6): 726-738.

Sturm, P., 2004. 3D-Color-Structure-Code. A new non-plainness island hierarchy. *In ICCSA 2004, International Conference on Computational Science and Its Applications.* Springer Press.

Suzuk, H., Toriwak, J., 1991. Automatic segmentation of head mri images by knowledge guided thresholding. *Computerized Medical Imaging and Graphics.* 15(4): 233-240.

Vovk, U., Pernus, F., Likar, B., 2004. MRI intensity inhomogeneity correction by combining intensity and spatial information, *Physics in Medicine and Biology*. 49: 4119-4133.

Wells III, W. M., Grimson, W. E. L., Kikinis, R. Jolesz, F. A. 1996. Adaptive segmentation of MRI data. *IEEE Trans on Medical Imaging*. 15(4): 429-442.

Zhang, Y. Y., Brady, M., Smith, S., 2001. Segmentation of brain MR images through a hidden markov random field model and the expectation-maximization algorithm. *IEEE Trans on Medical Imaging*. 20(1): 45-57.